PHYSICAL REVIEW A **80**, 053409 (2009)

State selection in nonresonantly excited wave packets by tuning from nonadiabatic to adiabatic interaction

Nina Owschimikow,[1] Burkhard Schmidt,[2,*] and Nikolaus Schwentner[1,†]
[1]*Institut für Experimentalphysik, Freie Universität Berlin, Arnimallee 14, 14195 Berlin, Germany*
[2]*Institut für Mathematik, Freie Universität Berlin, Arnimallee 6, 14195 Berlin, Germany*
(Received 10 September 2009; published 11 November 2009)

We show for rotational alignment of diatomic molecules that the crossover from nonadiabatic to adiabatic limits is well described by a convolution of excitation pulse envelope and sinusoidal molecular response and that it takes place in a uniform way in the region between 0.1 and 1 for the ratio of pulse duration to rotational period. In a nonresonant Raman-type excitation, this crossover is used to manipulate the J composition of a rotational wave packet with respect to the initial thermal distribution. By optimizing the duration of a single pulse, arbitrarily narrow distributions at low J levels can be formed. A double-pulse excitation, where a longer second pulse acts as a selective dump pulse, allows to prepare nonthermal distributions centered at high J values. With the alignment signal on top of an isotropic background, experimental techniques sensitive to the induced anisotropy are optimally suited for implementation. To demonstrate the efficiency of the method, numerical simulations are carried out for rotational alignment in $^{14}N_2$ at various experimentally relevant laser intensities. The scheme is transferable to quantum systems with a significant variation in transition frequencies between subsequent levels.

DOI: 10.1103/PhysRevA.80.053409 PACS number(s): 42.50.Hz, 33.80.−b, 42.50.Md

I. INTRODUCTION

The generation and manipulation of quantum wave packets by laser pulses has been an active field of research for many years [1,2]. A quantum wave packet with its characteristic recurrences in time is formed by coherently exciting a superposition of a finite number of quantum states with discrete frequencies, which persist in coherent motion after the excitation pulse is turned off [3,4]. To initiate this post-pulse coherent dynamics, the perturbation of a set of quantum states by the laser field must be short compared to the characteristic transition frequencies. In this case, termed nonadiabatic, the coupling of states at the time of the excitation imprints a common phase on the subsequent evolution, and the laser field is turned off too fast to allow for complete elimination of the induced polarization. Nonadiabatically excited wave packets can be manipulated in a number of ways by applying shaped pulses or pulse trains to achieve constructive or destructive interferences and thus to amplify or to erase the coherent post-pulse motion [5,6]. In contrast, for an adiabatic interaction, the perturbation of the quantum system by the laser proceeds on a time scale slow enough for every state of the system to evolve into the adiabatically correlated state and to return fully reversibly back into its initial condition.

In case of resonantly excited transitions, the laser frequency distribution serves as parameter to address a specific set of quantum states and to determine the frequency content of a wave packet. For nonresonantly excited wave packets, however, to achieve spectral selectivity appears more challenging. In this paper, we propose a method to shape the composition of nonresonantly excited wave packets by using the pulse duration as an active tool for selectively tuning the interaction from nonadiabatic to adiabatic for a subset of quantum states. This method is applicable in the case of transition frequencies varying strongly and monotonically between subsequent quantum states such as the electronic term energies in Rydberg progressions [7,8] or the rotational energies of molecules. We focus on the rotational alignment of diatomic molecules by linearly polarized laser pulses with energies scaling with the rotational quantum number J, as $J(J+1)$, and the transition frequencies restricted to $\Delta J = \pm 2, 0$ according to the Raman selection rules in nonresonant excitation. Nonresonant excitation is the method of choice in the study of rotational wave packets, as only laser sources offer sufficient time resolution. Numerical simulations of the degree of post-pulse alignment versus the ratio of pulse duration to rotational frequency reveal a unique transition from nonadiabatic to adiabatic with increasing ratio. This means that for a fixed pulse length, low J states lie on the nonadiabatic and high J levels on the adiabatic side, with the border shifting to higher J for shorter pulses. We illustrate that, starting from a thermal ensemble, long pulses can be used to excite the slow and thus low-energy part of the J distribution. In a consequent extension, we demonstrate that a combination of a short pump and a long dump pulse enables to select the high energetic part. The dump pulses therefore can be shaped to quench nonadiabatically only the cold side of the distribution generated by the pump, leaving the dynamics of rotationally hot molecules unchanged.

The efficiency of the method is demonstrated by numerical simulations of nonadiabatically excited rotational alignment, which has been an object of intense research over the past two decades [9,10]. The parameters of the simulations are set to closely correspond to realistic experimental conditions, and the $^{14}N_2$ molecule was chosen to serve as a tutorial example, nitrogen being the work horse in many nonadiabatic alignment experiments [9]. The control of rotational

*burkhard.schmidt@fu-berlin.de
†nikolaus.schwentner@physik.fu-berlin.de

wave packets by pairs or trains of pulses has been studied, both theoretically [11–15] and experimentally [16–20]. Most of these efforts have been directed toward an optimization of the degree of alignment through shaped excitation pulses [21–23] or pulse trains [17]. Optimization of alignment by adiabatic turn-on of the laser pulse has been investigated in Refs. [24,25]. In contrast to previous studies, the present contribution deals with a selection of a particular subensemble of J states from a broad thermal ensemble. The annihilation of coherent rotational motion by an adequately timed dump pulse was demonstrated in Refs. [16,19] and it is as such contained in our more general two-pulse scheme. A rather specific modification of the composition of rotational wave packets has been achieved by selectively de-exciting molecules in even or odd rotational states, increasing the frequency spacing in the wave-packet spectrum by a factor of 2 [20]. Our contribution complements these methods by allowing to selectively excite coherent rotational dynamics in molecules residing in a particular band of the rotational distribution of a thermal ensemble. In this way, a nonthermal density packet with adjustable J composition can be created from a thermal ensemble.

II. THEORETICAL FRAMEWORK

In the intense alternating electric field of a linearly polarized laser pulse, the electronic shell of a molecule is deformed as the electrons follow the rapid oscillations of the laser field. While any interaction with a permanent dipole moment of the molecule is averaged out by the alternating field direction, a molecule with an anisotropy of polarizability seeks to minimize its energy by aligning the axis with maximal polarizability along the field direction. For a diatomic molecule, the anisotropic polarizability is defined as

$$\Delta\alpha = \alpha_{\parallel} - \alpha_{\perp}, \tag{1}$$

with the polarizability $\alpha_{\parallel}$ parallel to the molecular axis and the polarizability $\alpha_{\perp}$ perpendicular to the axis, where in an electronic Σ state, $\alpha_{\parallel} > \alpha_{\perp}$ generally holds. The potential the molecule experiences in a laser field far off from any resonance can, within the rotating wave approximation, be expressed as [26]

$$H_{\mathrm{ind}}(t) = -\frac{1}{4}\Delta\alpha E^2(t)\cos^2\theta - \frac{1}{4}\alpha_{\perp}E^2, \tag{2}$$

where E is the amplitude of the laser electric field, and θ is the angle between molecular axis and laser polarization direction. The $\cos^2\theta$ term in the energy favors an alignment of the molecular axis in the electric field direction. The Hamiltonian for the nonresonant molecule field interaction is the sum of the Hamiltonian of the free molecule $\hat{H}_0$ and the potential induced by the electric field $\hat{H}_{\mathrm{ind}}(t)$,

$$\hat{H}(t) = \hat{H}_0 + \hat{H}_{\mathrm{ind}}(t), \tag{3}$$

where

$$\hat{H}_0 = B\hat{J}^2 \quad \text{with} \quad \hat{H}_0|JM\rangle = BJ(J+1)|JM\rangle, \tag{4}$$

and $\hat{J}$ denoting the angular momentum operator, neglecting centrifugal distortion. B is the rotational constant and $|JM\rangle$ is a rotational eigenstate characterized by the angular momentum quantum number J and its projection onto the laser polarization direction M. Frequently, the parameters are collected in the dimensionless interaction strength $\Delta\omega(t) = \Delta\alpha E^2(t)/(4B)$. For the $^{14}N_2$ molecule in the vibrational ground state, one has $B/hc = 1.98\ \mathrm{cm}^{-1}$ [27] and $\Delta\alpha = 0.89\ \text{Å}^3$ [28] with a rotational revival time unit of $\tau_1 = \hbar/(2B) = 8.38$ ps. A laser pulse with a power density of 10 TW/cm^2 under these conditions translates into a $\Delta\omega$ of approximately 50.

A rotational quantum state of a molecule is usually expanded in terms of eigenstates of the free rotor $|J'M'\rangle$ as

$$|\Psi_{JM}(t)\rangle = \sum_{J'M'} c^{(JM)}_{J'M'}(t)|J'M'\rangle, \tag{5}$$

where the time dependence of the coefficients is accounting for the mixing of free rotor states during the pulse and after and where the initial conditions are given by $c^{(JM)}_{J'M'}(t=0) = \delta_{JJ'}\delta_{MM'}$.

In a realistic experiment, a thermal ensemble of molecules is studied and described by the density-matrix formalism, which was introduced to the field of alignment in Refs. [29,30]. The density matrix $\hat{\rho}$ for a system in a mixed state is defined as $\hat{\rho} = \Sigma_{JM} w(J)|\Psi_{JM}(t)\rangle\langle\Psi_{JM}(t)|$, which can be cast in $|JM\rangle$ representation as

$$\hat{\rho}(t) = \sum_{J'M'}\sum_{J''M''} \rho_{J'M'J''M''}(t)|J'M'\rangle\langle J''M''|, \tag{6}$$

with

$$\rho_{J'M'J''M''}(t) = \sum_{JM} w(J)[c^{(JM)}_{J''M''}(t)]^* c^{(JM)}_{J'M'}(t). \tag{7}$$

The statistical weight $w(J)$ for every $|\Psi_{JM}(t)\rangle$ state is determined from the multiplicity $w_I(J)$ of symmetric and antisymmetric nuclear-spin states, with I being the nuclear spin, and the rotational partition function according to

$$w(J) = \frac{w_I(J)(2J+1)e^{-BJ(J+1)/k_BT}}{\sum_J w_I(J)(2J+1)e^{-BJ(J+1)/k_BT}}, \tag{8}$$

where T denotes the rotational temperature and k_B being the Boltzmann constant. In units of k_B/B, the dimensionless temperature Θ for $^{14}N_2$ corresponds to 28 at 80 K and 105 at 300 K. The rotational distribution for the $^{14}N_2$ molecule is exemplified in Fig. 1(a) for 80 K, close to the liquefaction temperature of 77.4 K, and at room temperature. Due to the small spacing of rotational levels, a large number of states is populated even at low temperature, and for more massive molecules the number of populated states is even larger as the level spacing decreases with increasing molecular mass. ^{14}N being a boson with $I=1$, the homonuclear molecule $^{14}N_2$ displays two subspecies with symmetric and antisymmetric nuclear-spin states with $w_I^{\mathrm{even}} = (2I+1)(I+1)$ and $w_I^{\mathrm{odd}} = (2I+1)I$, which can exist exclusively in symmetric or antisym-

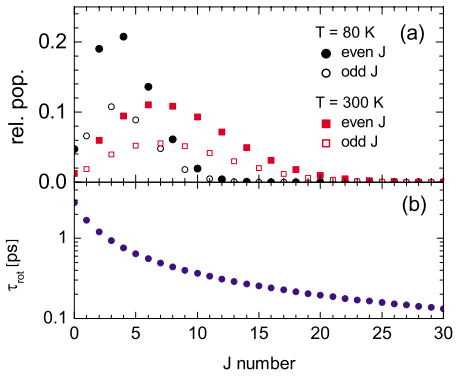

FIG. 1. (Color online) (a) Population of rotational levels for $^{14}N_2$ at 80 K (black symbols) and 300 K [red (gray) symbols]. ^{14}N being a boson with $I=1$, nuclear-spin statistics for homonuclear molecules requires the even J levels being twice more populated than the odd ones. (b) Semilogarithmic plot of rotational period τ_{rot} vs J quantum number.

metric rotational states due to stringent symmetry requirements for the total molecular wave function.

The time evolution of the density operator $\hat{\rho}$ is expressed in terms of the quantum Liouville–von Neumann equation,

$$\frac{d\hat{\rho}(t)}{dt} = -\frac{i}{\hbar}[\hat{H}_0 + \hat{H}_{\text{ind}}(t), \hat{\rho}], \tag{9}$$

where the initial density is chosen corresponding to a thermal ensemble [cf. Eq. (8)]. For adiabatic pulses, the electric field envelope can be considered as time independent, and the corresponding equations have solutions in the form of the so-called pendular states [26,31,32]. Analytical solutions of Eq. (9) exist for the impulsive and the classical limit [33]. For nonadiabatic pulses of finite duration, however, one has to resort to numerical evaluation of the rotational dynamics. Our numerical simulations of alignment dynamics were carried out by adapting a MATLAB code modeling the interaction of a diatomic molecule with a laser field with Gaussian pulse envelope, published as part of the WAVEPACKET 4.7 software package [34].

The quantity characterizing the degree of alignment in a $|\Psi_{JM}(t)\rangle$ state along the laser polarization direction is the quantum-mechanical expectation value $\langle\cos^2\theta\rangle_{JM}(t)$ of the squared cosine of the angle θ between the molecular axis and the polarization direction of the laser pulse. In $\langle\cos^2\theta\rangle_{JM}(t)$, the wave-packet dynamics originating from a coherent superposition of rotational states upon excitation of a pure state is contained. Though the alignment of quantum state-selected molecules has recently been demonstrated experimentally [35], separating molecules into specific quantum states remains a very demanding task [36], and thus with few exceptions, e.g., parahydrogen [37], the rotational dynamics of pure states is not observable under normal laboratory conditions. In an experiment, one observes a "density packet," resulting from averaging of densities rather than wave functions in the thermal ensemble. The dynamics of the ensemble is characterized by the ensemble-averaged squared alignment cosine denoted as $\langle\langle\cos^2\theta\rangle\rangle(t)$, which is expressed in terms of the density operator $\hat{\rho}(t)$ as

$$\langle\langle\cos^2\theta\rangle\rangle(t) = \text{Tr}\{\cos^2\theta\hat{\rho}(t)\}, \tag{10}$$

where Tr denotes the trace of the matrix product. For a randomly oriented ensemble of diatomic molecules, all angles of orientation of the molecular axis with respect to an external axis appear with equal probability, and the average of the squared orientation cosine amounts to $\langle\langle\cos^2\theta\rangle\rangle=1/3$. The coherent post-pulse alignment results in deviations to the positive as well as to the negative side around an average value larger than 1/3. Oscillations and the offset from 1/3 are contained in the off-diagonal and in the diagonal elements of the density matrix, respectively, which can easily be decomposed into these parts. In the diagonal elements, projecting a state $|JM\rangle$ onto itself, the population of the eigenstates $|JM\rangle$ is represented. The diagonal population part of the squared alignment cosine will be referred to as $\langle\langle\cos^2\theta\rangle\rangle_p$ following the convention of Ref. [29]:

$$\langle\langle\cos^2\theta\rangle\rangle_p(t) = \sum_{J'M'} \langle J'M'|\cos^2\theta|J'M'\rangle\rho_{J'M'J'M'}(t), \tag{11}$$

which is time dependent only as long as population is redistributed under the action of the external field. The $\Delta M=0$ selection rule for excitation with linearly polarized light leads to the value of $\langle\langle\cos^2\theta\rangle\rangle_p$, increasing beyond the isotropic value of 1/3 as for every additional J level reached in the rotational ladder climbing, the highest M quantum numbers, which have the smallest projection on the polarization axis, are not populated.

The coherence part of the squared alignment cosine is accordingly [29] expressed as

$$\langle\langle\cos^2\theta\rangle\rangle_c(t) = \sum_{\substack{J'\neq J'' \\ M'\neq M''}} \langle J'M'|\cos^2\theta|J''M''\rangle\rho_{J'M'J''M''}(t). \tag{12}$$

The off-diagonal matrix elements of $\hat{\rho}$ represent the coherences between different eigenstates and for a particular nonzero $\rho_{J'M'J''M''}$ oscillate at the beating frequency of the two eigenenergies. The coherence contribution $\langle\langle\cos^2\theta\rangle\rangle_c$ can by definition take on positive or negative values, depending on whether the direction of molecular axes at a particular instant in time tends to increase or to diminish the alignment with respect to the laser field direction. By definition, for all times one has $\langle\langle\cos^2\theta\rangle\rangle(t)=\langle\langle\cos^2\theta\rangle\rangle_p(t)+\langle\langle\cos^2\theta\rangle\rangle_c(t)$.

The alignment dynamics of the ensemble averaged $\langle\langle\cos^2\theta\rangle\rangle_p$ and $\langle\langle\cos^2\theta\rangle\rangle_c$ upon excitation of a thermal ensemble of $^{14}N_2$ at 80 K with a Gaussian laser pulse of 30 fs full width at half maximum (FWHM), well within the nonadiabatic limit up to $J=12$, is shown in Fig. 2(a). The increase in the population part during the pulse [red (gray) curve] shows the larger average alignment in field direction after the pulse. This increase amounts to typically only a fraction of a percent of the isotropic value. The ensemble displays post-pulse coherent rotational dynamics around this new equilibrium value with periodic revivals of alignment (black line), the details of which have been discussed extensively in the literature [38,39]. Large coherent alignment amplitudes just

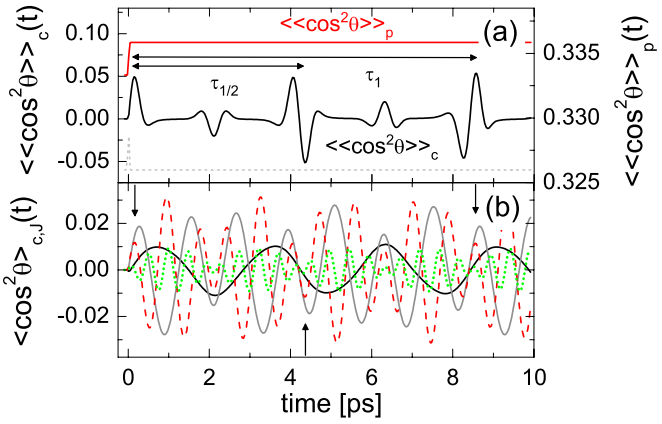

FIG. 2. (Color online) (a) Numerical simulation of nonadiabatic alignment in $^{14}N_2$ at 80 K upon excitation with a Gaussian pulse of 30 fs FWHM and an intensity of 5 TW/cm^2 (timing of pulse indicated by dashed line). The dynamics is split into the ensemble-averaged $\langle\langle\cos^2\theta\rangle\rangle_p(t)$ (solid red (gray) line) and $\langle\langle\cos^2\theta\rangle\rangle_c(t)$ (solid black line) parts. Times of half and first revivals are indicated as $\tau_{1/2}$ and τ_1, respectively. (b) Coherent oscillations $\langle\cos^2\theta\rangle_c(t)$ starting from the $J=0$ (black), $J=2$ (gray), $J=4$ [red (dashed)], and $J=8$ [green (dotted)] rotational states averaged over all M. The location of $\tau_{1/2}$ and τ_1 in the ensemble-averaged curve is indicated by vertical arrows.

after the pulse and at $\tau_{1/2}$ (4.19 ps) and τ_1 (8.38 ps) time delay after the first alignment peak are observable and, additionally, in between the smaller quarter revivals typical of homonuclear molecules. In Fig. 2(b), the coherent dynamics induced in the fractions of the ensemble originally occupying the $J=0$, 2, 4, and 8 rotational levels, averaged over all M numbers, are plotted separately. Individually, the curves display oscillations with large amplitude, with the frequency increasing with the rotational quantum number. Overall constructive interference, however, is realized only for a short-time interval around the full (τ_1) and half ($\tau_{1/2}$) revival times indicated by vertical arrows. The time evolution of $\langle\langle\cos^2\theta\rangle\rangle(t)$ is determined by the time evolution of the coefficients of the density matrix. After the termination of the pulse, the coefficients $\rho_{J'M'J''M''}(t)$ evolve according to

$$\rho_{J'M'J''M''}(t) = e^{-i(B/\hbar)[J''(J''+1)-J'(J'+1)](t-t_f)}\rho_{J'M'J''M''}(t_f), \tag{13}$$

where t_f is the time of the termination of the pulse and $t > t_f$. From the Wigner $3j$ formalism, it follows that the matrix elements in Eqs. (11) and (12) are nonzero only for $\Delta J = \pm 2, 0$ [40]. The time scale of the oscillations is thus determined by the beating frequencies between the coupled eigenstates. With the frequencies derived from Eq. (13) as $(4J+6)B/\hbar$ for a transition from J to $J+2$, the characteristic periods τ_r (J) are 2.79 ps, 1.19 ps, 0.69 ps, 0.44 ps, and 0.24 ps for the $J=0\rightarrow 2$, $J=2\rightarrow 4$, $J=4\rightarrow 6$, $J=8\rightarrow 10$, and $J=16\rightarrow 18$ transitions of the $^{14}N_2$ molecule, respectively [Fig. 1(b)].

III. SINGLE-PULSE EXCITATION

The efficiency of a Raman-type process, such as the nonresonant rotational excitation, generating molecular alignment in general depends quadratically on the applied laser intensity. However, the quadratic dependence in population of levels does not necessarily translate into a quadratic dependence of the squared cosine $\langle\langle\cos^2\theta\rangle\rangle$. In Fig. 3, the maximal amplitudes reached in numerical simulations of alignment in $^{14}N_2$ at 80 K by the ensemble-averaged expectation values $\langle\langle\cos^2\theta\rangle\rangle_p$ and $\langle\langle\cos^2\theta\rangle\rangle_c$ above their field-free values of 1/3 and zero, respectively, are plotted on a double-logarithmic scale. The population part represented by solid circles and solid lines very well follows a quadratic dependence over a wide range of intensities. The maximal amplitude reached by the coherence contribution $\langle\langle\cos^2\theta\rangle\rangle_c$ after the pulse equally well can be described by a linear dependence over a range of intensities up to 100 TW/cm^2, which corresponds to an interaction strength of $\Delta\omega \approx 500$ in dimensionless units. At higher power densities, both parts show a saturation behavior in the simulated alignment as they approach the limiting value of 1/2 [30] represented by the dotted horizontal line. However, the alignment in such high fields is competing with ionization, making this region inaccessible to alignment experiments. A closer inspection of the overlaid lines reveals that the intercepts at lines of constant intensity depend quadratically in the case of $\langle\langle\cos^2\theta\rangle\rangle_p$ and linearly in the case of $\langle\langle\cos^2\theta\rangle\rangle_c$ on the relative pulse intensities. Thus, for moderate intensities, the parameter defining the amplitudes of alignment reached by nonadiabatic excitation is the total energy contained in the laser pulse, confirming the findings of Ref. [41]. The same behavior was also noted for the classical limit [11].

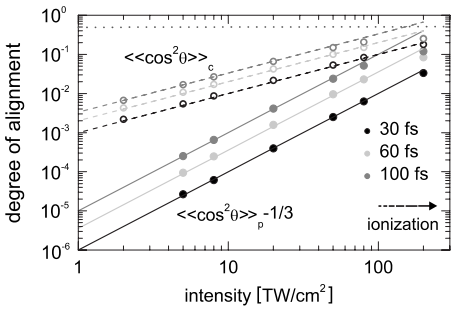

FIG. 3. Dependence of maximal deviation of post-pulse values of the ensemble-averaged population contribution $\langle\langle\cos^2\theta\rangle\rangle_p$ (solid circles) and coherent contribution $\langle\langle\cos^2\theta\rangle\rangle_c$ (open circles) from their respective isotropic values on laser-pulse intensity. The results of numerical simulations for alignment in $^{14}N_2$ upon excitation by Gaussian laser pulses with pulse durations of 30, 60, and 100 fs FWHM at a temperature of 80 K are plotted on a double-logarithmic scale. Solid lines represent overlaid quadratic dependences and dashed lines represent overlaid linear dependences. The limiting value of 1/2 is represented by the dotted horizontal line.

The relative insensitivity of the alignment amplitude to pulse length within the nonadiabatic limit can be qualitatively understood by picturing the post-pulse dynamics of a system that displays a sinusoidal response to a perturbation. Within the approximation of an undepleted two-level system, the response of a quantum state to a perturbation is described by a sinusoidal oscillation at the beating frequency ω of the eigenenergy of the two levels [42]. For a Gaussian laser pulse with finite duration, the convolution of the sinusoidal

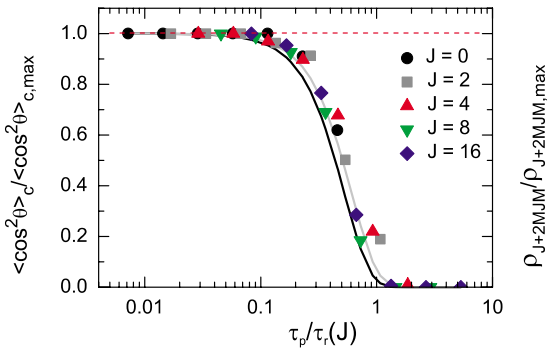

FIG. 4. (Color online) Semilogarithmic plot of the relative post-pulse coherent contribution $\langle\cos^2\theta\rangle_c$ from selected J states (colored symbols) normalized by the respective coherent contribution after the shortest pulse $\langle\cos^2\theta\rangle_{c,\max}$ vs ratio of Gaussian pulse FWHM to rotational period of the $J\rightarrow J+2$ transition. All pulses have identical integrated intensity. The solid lines represent the square of a convolution of the Gaussian excitation pulse envelope with a sinusoidal response (black) and the least-squares fit of a Gaussian function to the data (gray). The dashed horizontal line represents the limiting value of unity.

system response with the laser-pulse envelope can be evaluated analytically and leads to oscillatory post-pulse dynamics at the transition frequency ω_J with a maximal amplitude exponentially dampened by the squared ratio of rotational frequency to pulse length,

$$\rho_{J'M'J'+2M'}(t) \propto \sqrt{\frac{a_p}{\pi}}\int_{-\infty}^{\infty} e^{-a_p t'^2} \sin\omega_{J'}(t-t')dt'$$

$$= e^{-\omega_{J'}^2/4a_p} \sin\omega_{J'}t. \tag{14}$$

Up to a J-dependent amplitude, the convolution yields the magnitude of the off-diagonal elements of the density matrix $\rho_{J'M'J'+2M'}(t)$, and ω_J is the J-dependent frequency of the $J\rightarrow J+2$ rotational transition with $\omega_J=(4J+6)B/\hbar$ [43,44]. The pulse length is characterized by $a_p=4\ln 2/\tau_p^2$, with τ_p being the FWHM of the pulse envelope. Transforming the units into the dimensionless ratio of pulse FWHM to rotational period [Fig. 1(b)] by setting $\omega_J^2/4a_p=\pi^2/(4\ln 2)[\tau_p/\tau_r(J)]^2$, one arrives at a universal dependence

$$\rho_{J'M'J'+2M'}(t) \propto e^{-\pi^2/4\ln 2[\tau_p/\tau_r(J')]^2} \tag{15}$$

for all J levels plotted as black solid curve in Fig. 4. To show that this dependence really holds for coherent rotational dynamics, we numerically solve Eq. (9) for a range of pulse durations from 20 to 1280 fs FWHM. The transition from the nonadiabatic to the adiabatic limit obtained from the numerical simulations for rotational levels between $J=0$ and $J=16$ is shown in Fig. 4 as colored symbols. The simulated maximal post-pulse amplitude of the coherent contribution $\langle\cos^2\theta\rangle_c$ normalized by the amplitude $\langle\cos^2\theta\rangle_{c,\max}$ reached for the shortest pulse is plotted for each J versus the ratio of pulse length to the rotational period τ_r of the corresponding $J\rightarrow J+2$ transition. The variation in amplitudes with pulse length confirms the qualitative model of Eq. (14). A least-squares fit of a Gaussian dependence (gray curve) to the data results in a FWHM of 1.01 in dimensionless units compared to $4\ln 2/\pi(\approx 0.88)$ for the result of the convolution. Up to a ratio of 0.1 or the rotational period exceeding the pulse duration by at least a factor of 10, the relative values of $\langle\cos^2\theta\rangle_c$ remain close to unity for all J. Though the most efficient pulse appears to be a δ pulse, the decay in amplitude is slow enough to justify the assumption that in this region the alignment amplitude depends only on integrated pulse intensity. In the region around the flat top of the Gaussian, the interaction thus can be classified as nonadiabatic. In case of significant rotational ladder climbing, the limiting frequency for nonadiabatic interaction is the one of the highest excited transition. For ratios between 0.1 and 1, a pronounced decrease in amplitude appears, as the spread in phase accumulated during the pulse duration leads to a growing destructive interference between oscillations originating from the leading and the trailing edge of the pulse. Beyond a ratio of unity, and the pulse duration exceeding the rotational period, the amplitude of coherent post-pulse dynamics is reduced to zero. In this case, the fully adiabatic limit is approached.

It is remarkable that all J states follow the same decay on this dimensionless scale. For states separated by more than one order of magnitude in the time scale of their rotational period, there exists a completely adiabatic regime for the high-energy state and almost nonadiabatic behavior for the low-energy state. The behavior of rotational quantum states interacting with a laser pulse in the completely adiabatic and the completely nonadiabatic regimes has been investigated in Refs. [41,45]. Figure 4 together with Fig. 3 can be used to predict efficiencies of alignment for pulses with different lengths and for arbitrary temperatures by taking into account the proper statistical weight for every J state [Eq. (8)]. As the response to pulses of equal integrated intensity can be considered equal within the nonadiabatic limit, we exploit these properties and carry out all following simulations for pulses with identical energy content but different pulse length. Pulse duration and power densities are correlated with 20 fs, 40 fs, 80 fs, 160 fs, 320 fs, 640 fs, and 1280 fs FWHM laser-pulse duration corresponding to 64 TW/cm^2, 32 TW/cm^2, 16 TW/cm^2, 8 TW/cm^2, 4 TW/cm^2, 2 TW/cm^2, and 1 TW/cm^2, respectively, and to simplify the notation we will state only the pulse duration in the following.

In Fig. 5, the response to excitation with pulses of identical integrated intensity and different duration is exemplified by numerical simulations of $\langle\cos^2\theta\rangle_c$. The nonadiabatic limit of interaction is represented in Fig. 5(a) for dynamics starting from the $J=0$ rotational level upon excitation with laser pulses of 80 fs, 320 fs, and 640 fs FWHM. The pulse durations are short compared to the $\tau_r=2.79$ ps rotational period of the $J=0\rightarrow 2$ transition. The dynamics following the 80 fs and 320 fs excitation appears identical, and only for the 640 fs excitation pulse a small reduction in amplitude is observed. The crossover to adiabatic behavior is visible in numerical simulations for dynamics starting from initially $J=8$ in Fig. 5(b). With the same pulse parameters as above, large amplitude post-pulse oscillations appear only for the shortest excitation pulse of 80 fs FWHM, for 320 fs excita-

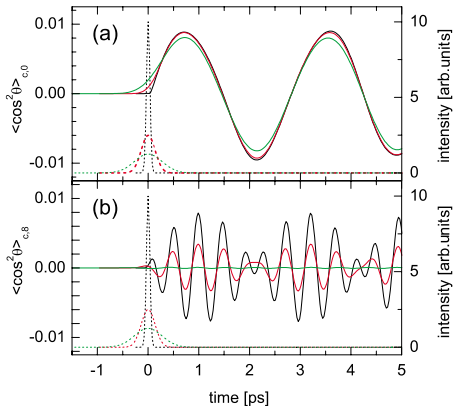

FIG. 5. (Color online) (a) Numerical simulation of $\langle \cos^2 \theta \rangle_c$ in $^{14}N_2$ starting from the $J=0$ rotational level upon excitation with Gaussian laser pulses with the same integrated intensity and a FWHM of 80 fs (solid black line), 320 fs [solid red (gray) line] and 640 fs [solid green (light gray) line]. The respective laser-pulse envelopes are represented by dashed lines. (b) Numerical simulation of alignment dynamics starting from the $J=8$ rotational level with pulse lengths and intensities as in (a).

tion the amplitude of coherent oscillations is much lower, and it is essentially reduced to zero for the longest pulse examined. The dominant time scale in this case is the 440 fs rotational period for the $J=8 \rightarrow J=10$ transition, bringing the 320 fs excitation pulse well into the crossover region from nonadiabatic to adiabatic and causing completely adiabatic behavior for the 640 fs FWHM pulse.

For short pulses, the amplitudes created during the pulse duration add up constructively and coherent motions persists after the pulse turn-off. For longer pulse durations, the polarization induced during the leading edge of the pulse is coherently removed with the trailing edge. Within the adiabatic approximation, the free rotor states evolve into pendular states [31], the eigenstates of the combined molecule-electric field system, and back into free rotor states, while the population of adiabatically corresponding levels is maintained at all times. Thus, for a long pulse, no net excitation is transferred to the system and alignment is high only during the pulse.

In the experimental observable $\langle\langle \cos^2 \theta \rangle\rangle$, all regimes of response can be contained depending on the number of populated rotational levels and laser-pulse duration. The rotational transitions, contributing to the post-pulse alignment, can be recovered from the Fourier transform of the time-dependent alignment trace. Using Eq. (13), the Fourier transform of $\langle\langle \cos^2 \theta \rangle\rangle(t)$ is expressed as

$$\begin{aligned}\langle\langle \cos^2 \theta \rangle\rangle(\omega) &= \int_{-\infty}^{\infty} e^{-i\hbar\omega t} \langle\langle \cos^2 \theta \rangle\rangle(t) dt \\ &= \sum_{\substack{J'M' \\ J''M''}} \rho_{J'M'J''M''}(t_f) \langle J'M' | \cos^2 \theta | J''M'' \rangle \\ &\quad \times \delta(BJ'(J'+1) - BJ''(J''+1) - \hbar\omega).\end{aligned} \tag{16}$$

With the appropriate selection rules $\Delta J=+2, \Delta M=0$ for the matrix elements of $\cos^2 \theta$, this expression for $\omega > 0$ is reduced to

$$\langle\langle \cos^2 \theta \rangle\rangle(\omega) = \sum_{J'} \delta(B(4J'+6) - \hbar\omega) \sum_{M'} \rho_{J'+2,M',J'M'}(t_f) \frac{\{(2J'+1)(2J'+5)[(J'+1)^2 - M'^2][(J'+2)^2 - M'^2]\}^{1/2}}{(2J'+1)(2J'+3)(2J'+5)}. \tag{17}$$

The Fourier transforms thus contain the contribution of the off-diagonal elements of the density matrix. The population part, being time independent after the pulse, does not contribute to the nonzero frequency part of the Fourier spectrum. The amplitudes with which individual coherences appear are determined by $\rho_{J' \pm 2M'J'M'}$ and the respective projections $\langle J'M' | \cos^2 \theta | J' \pm 2M' \rangle$ [40].

The crossover to adiabatic behavior with increasing pulse duration can be used to create a rotationally cold density packet within a thermal ensemble by selectively exciting only molecules in low rotational levels. Selective excitation in this context refers to the post-pulse dynamics, as the alignment induced in rotationally hot molecules during the pulse is adiabatically removed with the trailing edge. Fourier power spectra derived from numerically simulated post-pulse coherent dynamics by solving Eqs. (9) and (12) upon excitation of a thermal ensemble of $^{14}N_2$ at 80 K with laser pulses of 40 fs, 320 fs, and 1280 fs FWHM are displayed in Figs. 6(a)–6(c), respectively. The time traces are given in the corresponding insets. The Fourier spectrum upon excitation with the 40 fs pulse [Fig. 6(a)] spans about ten rotational transition frequencies, while the number of rotational levels significantly populated at a temperature of 80 K is about 11 [Fig. 1(a)]. The crossover to adiabatic behavior for this pulse length starts at $J=9$, at a fraction of 0.1 of the time scale of the $J=9 \rightarrow 11$ transition of 400 fs. Up to this level, the amplitudes of the individual rotational transitions are not masked by partial destructive interferences during the pulse duration. At room temperature, however, a large part of the populated rotational states would already fall into the crossover region to adiabatic behavior for 40 fs pulse duration (Fig. 1), and for the fully nonadiabatic limit pulse durations of 19 fs and shorter have to be used.

For the thermal ensemble at 80 K, the crossover is realized by increasing pulse durations beyond 40 fs. In Fig. 6(b), the Fourier spectrum recovered upon excitation with a pulse

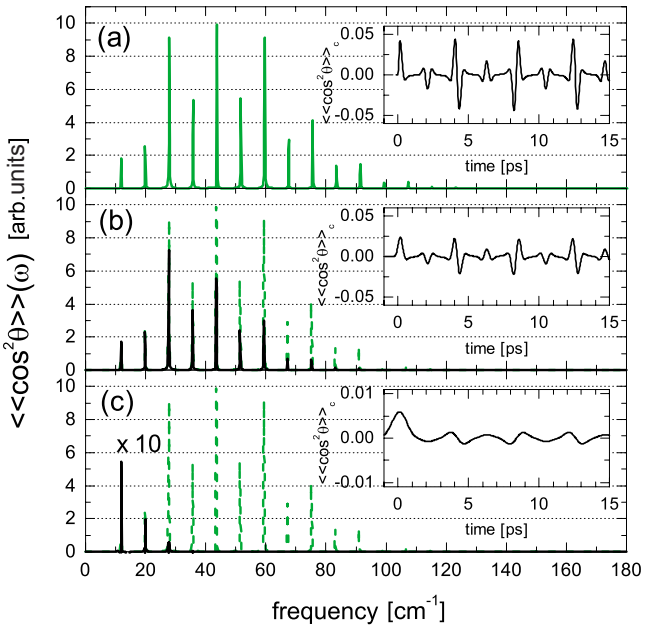

FIG. 6. (Color online) Fourier transforms of alignment traces from numerical simulations of $\langle\langle\cos^2\theta\rangle\rangle_c$ in $^{14}N_2$ at 80 K upon excitation with Gaussian laser pulses of 40 (a), 320 (b), and 1280 fs (c) FWHM (solid lines). The curve in (c) has been multiplied by a factor of 10. The green (dashed) line in (b) and (c) represents the Fourier transform upon 40 fs excitation. The respective $\langle\langle\cos^2\theta\rangle\rangle_c$ vs time is plotted in the insets.

of 320 fs FWHM (black line) is shown compared to the spectrum upon 40 fs excitation (dashed green line). The Fourier spectrum appears narrower and centered on the low-energetic side compared to the states populated in the thermal ensemble. The decrease in amplitude is significant starting from the peak representing the $J=2\rightarrow4$ rotational transition, and the amplitude is essentially reduced to zero above $J=8\rightarrow10$. The time trace in the inset of Fig. 6(b) shows broader revival structures compared to Fig. 6(a), also indicating a narrower frequency distribution. Extending the pulse duration further, the frequency content of the post-pulse dynamics can be narrowed even more, as is exemplified in Fig. 6(c) for a pulse of 1280 fs FWHM. Here, the $J=0\rightarrow2$ transition is dominating in the post-pulse dynamics, and all frequencies above $J=2\rightarrow4$ are completely suppressed. Note that the Fourier spectrum in Fig. 6(c) has been multiplied by a factor of 10 for better visibility compared to the dashed green (thermal) spectrum. It is thus not the thermal ensemble of molecules being rotationally cooled by a long pulse but rather the periodic dynamics is restricted to molecules in low rotational states. The small amplitude of coherent post-pulse oscillations (inset) is due to the low statistical weight of the contributing levels in the thermal ensemble. Characteristic of the adiabatic limit is the high amplitude of alignment during the pulse, which is not any more recovered in the post-pulse oscillations. The revival features in the time trace of Fig. 6(c) compared to Fig. 6(b) appear still broader; the time scale of the beating pattern, however, is similar in all cases, as it is governed by the largest common divisor of the rotational periods, i.e., $2B$ or 8.38 ps. In the extreme case, for excitation with pulses significantly exceeding the $J=1\rightarrow3$ characteristic time in FWHM, only the $J=0\rightarrow2$ transition will contribute and a crossover from a $\hbar/(2B)$ to a $\hbar/(6B)$ revival period will appear [37]. For experimental methods insensitive to an isotropic background, such as optical Kerr effect [37,46] or transient grating [20,47] detection, applying a long pulse serves to selectively monitor the coherent dynamics of rotationally cold molecules within thermal surroundings.

IV. DOUBLE-PULSE EXCITATION

In the previous section, we discussed how a long pulse serves to prepare a J density-packet distribution centered at low J. In this section, we introduce a scheme to shift the J distribution to high J. A first pulse excites a wide range of rotational transitions and now an appropriately designed second pulse has to eliminate the low J part.

Constructive and destructive interferences in rotational wave packets induced by a pair or train of laser pulses are well known from extensive studies in the literature. As in the rotational wave-packet nuclei are moving rather than electrons, the fast oscillations of the electric field within the laser-pulse envelope are averaged out within the rotating wave approximation, and the only control parameter is the timing of the second pulse with respect to the first one [48]. To achieve destructive interference, the dump pulse has to be applied at half a revival time past the pump pulse, corresponding to 4.19 ps or the root of $\langle\langle\cos^2\theta\rangle\rangle_c$ at the half revival time for $^{14}N_2$. The density packet of the first pulse evolves up to the negative antialignment indicated by $\tau_{1/2}$ in Fig. 2(b), while the second pulse generates the alignment maximum visible in Fig. 2(b) just after $t=0$. Both traces are mirror images of each other and in the superposition they cancel.

For the destructive interference to take place, it is not necessary that the dump pulse be identical to the pump pulse. Pulses within the nonadiabatic limit create an almost identical response in a particular rotational state (Fig. 4) and therefore destructive interference can be achieved by applying a dump pulse differing in duration from the pump pulse. In Fig. 7, the effect of dump pulses of various duration, following the excitation with a 40 fs pump pulse, is quantified relative to the rotational period of a particular excited $J\rightarrow J+2$ transition. The maximal amplitude of $\langle\cos^2\theta\rangle_c$ after the dump pulse normalized by the maximal post-pulse $\langle\cos^2\theta\rangle_c$ after the pump pulse is plotted as colored symbols versus the ratio of dump FWHM to rotational period for a range of J levels between 0 and 16. The curve gives the efficiency of de-excitation for a particular ratio of pulse length to rotational period and thus can be used to predict efficiencies of dump pulses of various lengths for arbitrary temperatures. As for the dependence of the degree of alignment on pump duration shown in Fig. 4, the curve shows two distinct regimes with nonadiabatic and adiabatic behaviors and between those a crossover region covering one order of magnitude in pulse duration. Once more, a remarkable common behavior for all J is observable. As for the pump case, the nonadiabatic limit extends up to a pulse width of 10% of the rotational period, in this region maximal destructive interference is achieved.

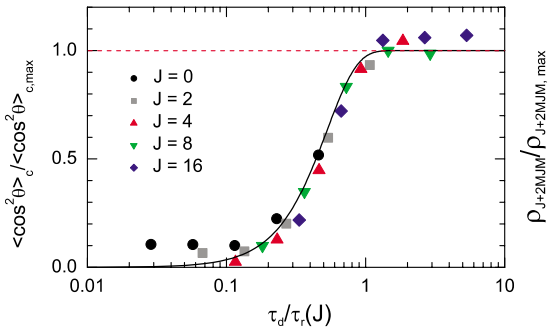

FIG. 7. (Color online) Semilogarithmic plot of the relative coherent contribution $\langle\cos^2\theta\rangle_c$ after the dump pulse for nonadiabatic dynamics starting from selected J stated normalized by $\langle\cos^2\theta\rangle_{c,\max}$ after the pump vs ratio of Gaussian pulse FWHM of dump pulse to rotational period of the $J\rightarrow J+2$ transition. All pulses have equal integrated intensities. The solid black curve represents the dependence of amplitude on dump pulse duration according to Eq. (19). The limiting value of unity is represented by the dashed horizontal line.

The fully adiabatic region sets in at pulse durations equal to the rotational period, where the presence of the dump pulse does not affect the degree of alignment. The dependence can be qualitatively described by the model of a convolution of Gaussian pulse with sinusoidal response. Introducing a second pulse shifted in time by the half revival time $\tau_{1/2}$, the convolution can be written and analytically solved as

$$\rho_{J'+2M'J'M'}(t) \propto \int_{-\infty}^{\infty} \left[\sqrt{\frac{a_p}{\pi}} e^{-a_p t'^2} \sin \omega_{J'}(t-t') + \sqrt{\frac{a_d}{\pi}} e^{-a_d t'^2} \sin \omega_{J'}(t+\tau_{1/2}-t') \right] dt' = (e^{-\omega_{J'}^2/4a_p} - e^{-\omega_{J'}^2/4a_d}) \sin \omega_{J'} t. \quad (18)$$

Here the pump and dump pulse durations are characterized by $a_p = 4 \ln 2/\tau_p^2$ and $a_d = 4 \ln 2/\tau_d^2$, respectively, and the rotational transition frequency $\omega_J = (4J+6)B/\hbar$ as in Eq. (14). In case of a nonadiabatic pump, the first exponential tends to unity, and the maximal post-pulse amplitude of $\rho_{J'+2M'J'M'}(t)$, resulting from the interference of dynamics excited by the pair of pulses, is accordingly expressed as

$$\rho_{J'+2M'J'M'} \propto 1 - e^{-\pi^2/4 \ln 2[\tau_d/\tau_r(J')]^2}. \quad (19)$$

This curve is plotted in Fig. 7 as solid black line and appears to very well describe the dependence of amplitudes on dump pulse duration. The relatively large scatter of data for different J states in the full simulation is due to small phase shift appearing between the levels of the three-dimensional rotor [19]. Varying the timing of the dump pulse can optimize the interaction with a particular state, for the three-dimensional rotor, however, there exists no zero-effect pulse pair with which perfect destructive interference for all levels can be achieved. The effect of optimized dump pulses on dynamics in the $J=0$ and $J=8$ rotational levels is shown in Fig. 8. The timing of the dump pulses has been chosen to optimize the

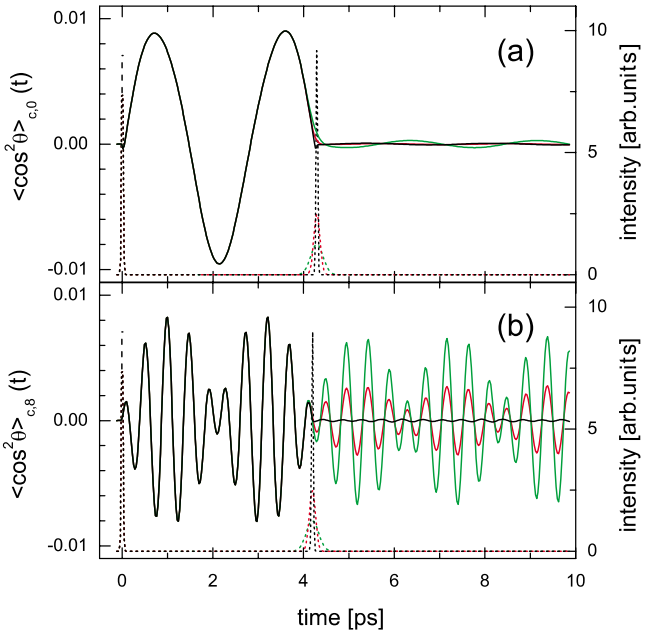

FIG. 8. (Color online) $\langle\cos^2\theta\rangle_c$ in $^{14}N_2$ starting from the $J=0$ rotational level upon excitation with a pump pulse of 40 fs and a dump pulse at a delay of 4.29 ps of 40 fs (solid black line), 320 fs (solid red (gray) line), and 640 fs [solid green (light gray) line] FWHM. The respective laser-pulse envelopes are represented by dashed lines. (b) Numerical simulation of alignment dynamics starting from the $J=8$ rotational level with pulse lengths and intensities as in (a). The time delay of the dump pulse is 4.2 ps.

destructive interference in the particular state. In Fig. 8(a), dump pulses of 40, 320, and 640 fs FWHM are applied after excitation with a 40 fs pump pulse. For this rotational transition, all these dump pulse durations are well below the adiabatic limit and, consequently, act almost equally on the dynamics. The 40 fs and 320 fs dump pulses essentially reduce the post-pulse oscillation amplitude to zero, while small amplitude oscillations are observed for the 640 fs dump pulse, indicating the onset of crossover to the adiabatic limit. With a $\tau_r = 440$ fs characteristic time for the $J=8\rightarrow 10$ rotational transition, the 320 fs and 640 fs FWHM dump pulses are well within the crossover region to adiabatic behavior. This is demonstrated in Fig. 8(b), displaying post-pulse coherent oscillations, starting from the $J=8$ rotational level. The 40 fs dump pulse erases the oscillations, while large amplitude dynamics is observable after the 320 and 640 fs dump pulses. The presence of a slowly varying field thus does not affect the coherent dynamics. Naturally, the fixed phase relation, giving rise to coherent oscillatory motion, existing before the application of the adiabatic field persists also after its turn-off.

For a thermal ensemble with a distribution in J, the effect of a dump pulse of fixed duration thus changes over the J spectrum. In Fig. 9(a), the Fourier power spectrum for numerically simulated destructive interference in a thermal ensemble of $^{14}N_2$ at 80 K upon the application of an identical pair of pump and dump laser pulses of 40 fs FWHM is plotted. The timing of the dump pulse was chosen to minimize

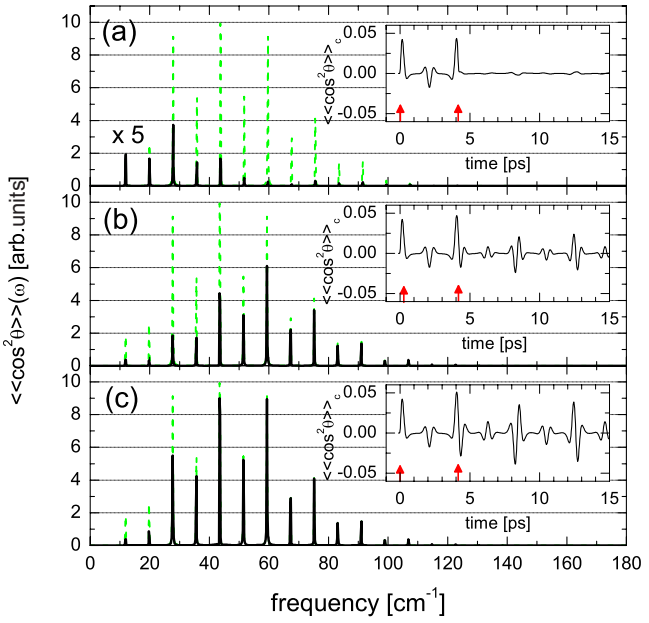

FIG. 9. (Color online) Fourier transforms of alignment traces from numerical simulations of $\langle\langle\cos^2\theta\rangle\rangle_c$ in $^{14}N_2$ at 80 K upon the application of a pair of Gaussian laser pulses of 40 fs duration for the pump and 40 (a), 320 (b), and 640 fs (c) FWHM (solid black lines) for the dump pulse delayed by 4.195 ps. The curve in (a) has been multiplied by a factor of 5. The green (dashed) spectra represent the Fourier transform upon excitation with only a single 40 fs FWHM pump pulse. The respective $\langle\langle\cos^2\theta\rangle\rangle_c$ vs time is plotted in the insets with the timing of the pulses indicated by vertical arrows.

the amplitude of post-pulse oscillations (inset). For comparison, the Fourier spectrum resulting from excitation with a 40 fs pump pulse (Fig. 6) is plotted as dashed green line. The symmetric dump pulse of Fig. 9(a) removes the bulk of the spectrum from the coherent dynamics, while in the wings small contributions are surviving. Note, however, that for better comparison of shape, the black spectrum was multiplied by a factor of 5 and thus in the plot appears overly large. The destructive interference in the different spectral regions can be further optimized by slight changes in the timing of the dump pulse [19]. From the discussion in the previous section, it follows that all pulses that contain the same energy but differ in duration have the same effect in coherently exciting a rotational wave packet, as long as they can be considered nonadiabatically short for the J set considered. Consequently, also a dump pulse must only be equal in the energy content to coherently de-excite the wave packet, however, only within the nonadiabatic limit. Now we proceed to violate this condition for a subset of J levels. In Fig. 9(b), the effect on the Fourier spectrum of a dump pulse equal in timing and energy content to the case of Fig. 9(a) but with a pulse duration of 320 fs FWHM is plotted. In the time trace, the coherent oscillations persist after the dump pulse (inset), however, with an amplitude that appears much reduced. The Fourier transform of the trace reveals that the spectrum after the dump pulse, represented by the black line, is lacking the low-energy part compared to the single-pulse case (dashed green line). Figure 9(c) displays the Fourier transform of the oscillations after the application of a 640 fs FWHM dump pulse. This pulse, as expected, appears to affect only the lowest J levels.

Long dump pulses thus interact selectively with the red part of the spectrum. Indeed, destructive interference is achieved irrespectively of the duration of the dump pulse as long as it is within the nonadiabatic limit, which is exactly true for the red wing of the rotational distribution. Rotational transitions for which the dump pulse is long enough to interact adiabatically, however, are not affected by its presence. As a result, the wave-packet spectrum after the application of an asymmetric pair of pump and dump pulses appears shifted to higher energies compared to the original case. The shift is not due to heating but rather due to selective de-excitation of the red wing of the wave-packet spectrum back to the original isotropic distribution. Tuning the pulse width of the dump pulse allows to control the limits of de-excitation and to generate narrow nonthermal wave-packet spectra. The large crossover region form nonadiabatic to adiabatic, however, demands to sacrifice large amplitudes in case spectral purity is required.

V. CONCLUSIONS

We demonstrated that adapting the pulse duration in nonresonant excitation of wave-packet states can serve as a tool to achieve spectral selectivity otherwise not permitted by the nonresonant nature of the process. For a quantum system with transition frequencies strongly increasing with the quantum number, increasing the excitation pulse length leads to a selective excitation of the low-energetic side of the spectrum, as higher lying levels are adiabatically transferred back into their original state. In double-pulse experiments, the length of the second (dump) pulse can be adjusted to selectively eliminate the red wing of the spectrum by tuning it into the adiabatic limit for the blue wing. This effect was demonstrated by numerically calculating spectrally controlled destructive interference in nonresonantly excited rotation of diatomic molecules. The J composition of the resulting alignment signal may be far from the temperature of the environment. With both schemes together, low J and high J rotational density packets can be designed. In this way, effects of nonequilibration of rotational and translational degrees of freedom, as they occur, for example, in typical molecular-beam expansion experiments, can be studied in a controlled way. The selectivity of the method depends on the nonequidistant spacing of quantum levels and is expected to increase with increasing level spacing, e.g., for rotational wave packets in O_2 or H_2. Note, however, that in these approaches of shaping the spectra of coherent oscillations, no significant population transfer between states is involved but rather the coherent rotational motion is restricted to a certain subpopulation, with the bulk of molecules forming an isotropic thermal background. From the viewpoint of experiments, it is thus favorable to employ a technique only sensitive to deviations from isotropy such as, e.g., the detection of time-dependent changes in birefringence in an optical Kerr effect or transient grating experiment. Shaping of rotational wave packets in this context could be used to study state-dependent alignment decay rates or to remove a dominant

low-energy contribution to an alignment signal. Additionally, we point out that the approach is not limited to the case of rotational excitation but can be extended to those cases of wave-packet dynamics for which a transition from adiabatic to nonadiabatic pulse length is permitted by the experiment and energy spacings between levels vary significantly, as it is the case, e.g., in Rydberg states.

ACKNOWLEDGMENTS

The authors are indebted to F. Königsmann, Dr. R. Püttner, and especially M. Héjjas for fruitful discussions and scientific insight. Financial support from Deutsche Forschungsgemeinschaft via Sonderforschungsbereich 450 is gratefully acknowledged.

[1] D. J. Tannor, *Introduction to Quantum Mechanics: A Time-Dependent Perspective* (University Science Books, Sausalito, 2007).
[2] K. Ohmori, Annu. Rev. Phys. Chem. **60**, 487 (2009).
[3] R. W. Robinett, Phys. Rep. **392**, 1 (2004).
[4] I. S. Averbukh and N. F. Perelman, Phys. Lett. A **139**, 449 (1989).
[5] M. Dantus and V. V. Lozovoy, Chem. Rev. **104**, 1813 (2004).
[6] M. Shapiro and P. Brumer, Rep. Prog. Phys. **66**, 859 (2003).
[7] J. Parker and C. R. Stroud, Phys. Rev. Lett. **56**, 716 (1986).
[8] J. A. Yeazell, M. Mallalieu, and C. R. Stroud, Phys. Rev. Lett. **64**, 2007 (1990).
[9] T. Seideman and E. Hamilton, Adv. At., Mol., Opt. Phys. **52**, 289 (2005), and references therein.
[10] H. Stapelfeldt and T. Seideman, Rev. Mod. Phys. **75**, 543 (2003), and references therein.
[11] M. Leibscher, I. S. Averbukh, and H. Rabitz, Phys. Rev. Lett. **90**, 213001 (2003).
[12] M. Spanner, E. A. Shapiro, and M. Ivanov, Phys. Rev. Lett. **92**, 093001 (2004).
[13] O. Atabek, C. M. Dion, and A. B. Yedder, J. Phys. B **36**, 4667 (2003).
[14] J. Ortigoso, Phys. Rev. Lett. **93**, 073001 (2004).
[15] D. Sugny, A. Keller, O. Atabek, D. Daems, C. M. Dion, S. Guerin, and H. R. Jauslin, Phys. Rev. A **72**, 032704 (2005).
[16] K. F. Lee, D. M. Villeneuve, P. B. Corkum, and E. A. Shapiro, Phys. Rev. Lett. **93**, 233601 (2004).
[17] C. Z. Bisgaard, M. D. Poulsen, E. Peronne, S. S. Viftrup, and H. Stapelfeldt, Phys. Rev. Lett. **92**, 173004 (2004).
[18] V. G. Stavros, E. Harel, and S. R. Leone, J. Chem. Phys. **122**, 064301 (2005).
[19] K. F. Lee, E. A. Shapiro, D. M. Villeneuve, and P. B. Corkum, Phys. Rev. A **73**, 033403 (2006).
[20] S. Fleischer, I. S. Averbukh, and Y. Prior, Phys. Rev. Lett. **99**, 093002 (2007).
[21] E. Hertz, A. Rouzee, S. Guerin, B. Lavorel, and O. Faucher, Phys. Rev. A **75**, 031403(R) (2007).
[22] D. Pinkham, K. E. Mooney, and R. R. Jones, Phys. Rev. A **75**, 013422 (2007).
[23] C. Horn, M. Wollenhaupt, M. Krug, T. Baumert, R. de Nalda, and L. Banares, Phys. Rev. A **73**, 031401(R) (2006).
[24] J. G. Underwood, M. Spanner, M. Y. Ivanov, J. Mottershead, B. J. Sussman, and A. Stolow, Phys. Rev. Lett. **90**, 223001 (2003).
[25] B. J. Sussman, J. G. Underwood, R. Lausten, M. Y. Ivanov, and A. Stolow, Phys. Rev. A **73**, 053403 (2006).
[26] B. Friedrich and D. Herschbach, J. Phys. Chem. **99**, 15686 (1995).
[27] G. Herzberg, *Molecular Spectra and Molecular Structure. I. Spectra of Diatomic Molecules* (Krieger, Malabar, FL, 1989).
[28] J. O. Hirschfelder, C. F. Curtiss, and R. B. Bird, *Molecular Theory of Gases and Liquids* (Wiley, New York, 1954).
[29] S. Ramakrishna and T. Seideman, Phys. Rev. Lett. **95**, 113001 (2005).
[30] S. Ramakrishna and T. Seideman, J. Chem. Phys. **122**, 084502 (2005).
[31] B. Friedrich and D. Herschbach, Phys. Rev. Lett. **74**, 4623 (1995).
[32] M. Leibscher and B. Schmidt, Phys. Rev. A **80**, 012510 (2009).
[33] M. Leibscher, I. S. Averbukh, and H. Rabitz, Phys. Rev. A **69**, 013402 (2004).
[34] B. Schmidt and U. Lorenz (2009), WAVEPACKET 4.7: A program package for quantum-mechanical wavepacket propagation and time-dependent spectroscopy; available via http://wavepacket.sourceforge.net
[35] L. Holmegaard, J. H. Nielsen, I. Nevo, H. Stapelfeldt, F. Filsinger, J. Küpper, and G. Meijer, Phys. Rev. Lett. **102**, 023001 (2009).
[36] S. Y. T. van de Meerakker, H. L. Bethlem, and G. Meijer, Nat. Phys. **4**, 595 (2008).
[37] F. Königsmann, M. Fushitani, N. Owschimikow, D. T. Anderson, and N. Schwentner, Chem. Phys. Lett. **458**, 303 (2008).
[38] T. Seideman, Phys. Rev. Lett. **83**, 4971 (1999).
[39] F. Rosca-Pruna and M. J. J. Vrakking, Phys. Rev. Lett. **87**, 153902 (2001).
[40] A. R. Edmonds, *Angular Momentum in Quantum Mechanics* (Princeton University, Princeton, 1960).
[41] R. Torres, R. de Nalda, and J. P. Marangos, Phys. Rev. A **72**, 023420 (2005).
[42] J. I. Steinfeld, *Molecules and Radiation: An Introduction to Modern Molecular Spectroscopy*, 2nd ed. (Dover, Mineola, NY, 2005).
[43] B. Lavorel, O. Faucher, M. Morgen, and R. Chaux, J. Raman Spectrosc. **31**, 77 (2000).
[44] M. Morgen, W. Price, P. Ludowise, and Y. Chen, J. Chem. Phys. **102**, 8780 (1995).
[45] J. Ortigoso, M. Rodriguez, M. Gupta, and B. Friedrich, J. Chem. Phys. **110**, 3870 (1999).
[46] V. Renard, M. Renard, S. Guerin, Y. T. Pashayan, B. Lavorel, O. Faucher, and H. R. Jauslin, Phys. Rev. Lett. **90**, 153601 (2003).
[47] Y. Mairesse, D. Zeidler, N. Dudovich, M. Spanner, J. Levesque, D. M. Villeneuve, and P. B. Corkum, Phys. Rev. Lett. **100**, 143903 (2008).
[48] Y. X. Li, P. Liu, S. T. Zhao, Z. A. Zeng, R. X. Li, and Z. Z. Xu, Chem. Phys. Lett. **475**, 183 (2009).